

Design of Ultra-Broadband Antireflection Coatings Utilizing Integrated Moth-Eye Structures for Multi-Junction Device Applications

Emmett E. Perl¹, Chieh-Ting Lin¹, William E. McMahon², John E. Bowers¹, and Daniel J. Friedman²

¹University of California at Santa Barbara, Santa Barbara, CA, 93106, USA

²National Renewable Energy Laboratory, Golden, CO, 80401, USA

Abstract — Ultra-broadband Antireflection Coatings (ARCs) are essential to realizing the potential efficiency gains of four-junction photovoltaic devices that absorb to longer wavelengths than state-of-the-art three-junction cells. In this work, we examine a novel design that integrates a nanostructured antireflection layer with a multilayer ARC. Using optical models, we find that this hybrid approach can reduce the reflected AM1.5D power by 10-45 W/m² compared to conventional thin-film ARCs. A hybrid ARC is designed and fabricated on a sample consisting of approximately 1 μm of indium gallium phosphide (InGaP) on gallium arsenide (GaAs). For the hybrid coating, we measure a reflection loss of just 23.9 W/m² corresponding to less than a 3% power reflection.

Index Terms — biomimetics, III-V semiconductor materials, nanophotonics, optical films, photovoltaic cells, solar energy.

I. INTRODUCTION

For nearly two decades, multi-junction solar cells have had the highest efficiencies of all photovoltaic technologies. Current three-junction (3-J) architectures have achieved efficiencies as high as 44.0% under concentration, and the development of four-junction (4-J) devices will put the industry within striking distance of attaining 50.0% conversion efficiency. [1][2]

State-of-the-art cells are typically based on III-V materials, which reflect around 30% of incident light due to the high index of refraction of these compounds. A standard 2-layer antireflection coating (ARC) is usually sufficient to reduce the impact of reflections for most 3-J devices, even with a passband that does not span the solar spectrum.

This is the case for germanium based 3-J devices because high IR reflectivity will not affect a 0.66-eV lower junction as long as it remains oversupplied with photons. For devices that use a bottom junction with a bandgap closer to 1.0-eV, IR requirements are not as intense since the cell will absorb a much narrower range of wavelengths. [3]

However, 4-J designs incorporating an additional low bandgap material are more constrained and have intense requirements for infrared ARC performance. These devices will require ARCs with consistently low power reflection over a wavelength range from about 300-1800 nm. [4][5]

One common approach to reduce reflections over a 2-layer coating is to deposit more ARC layers onto the sample. While these multilayer designs can outperform a 2-layer ARC, it is difficult to significantly reduce the average reflectance to less than 5% over the relevant 4-J wavelength range using

commonly available materials. This reflection will correspond to a loss in absolute cell efficiency of 1-2% for a four-junction photovoltaic device.

An alternative approach makes use of antireflective nanostructures, which consist of sub-wavelength protrusions originally discovered on the surface of a moth-eye to minimize visibility to predators. If these nanostructures are tapered, incoming light will see a smooth gradient in the effective index of refraction. With no abrupt interfaces, Fresnel reflections are greatly reduced and near-zero reflectance over a broad range of wavelengths and angles is possible. [6][7]

However, these anti-reflective nanostructures are difficult to integrate onto active photovoltaic devices without introducing additional loss mechanisms. Direct patterning of the active device is usually coupled with cell damage. To avoid this, it is necessary to integrate the moth-eye nanostructures into a transparent and electrically isolated layer that is at least a few hundred nm thick. However, finding a suitable material that is index-matched to the active layers which will also not absorb a significant amount of incoming light is very difficult. [8]

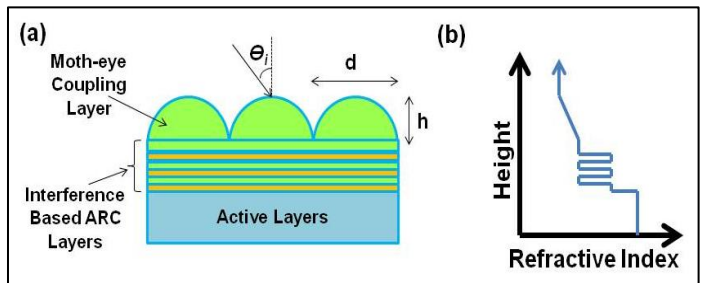


Fig. 1. (a) Diagram of the hybrid moth-eye design. (b) Effective index of refraction vs. height for the full antireflective structure.

Here, we report on a novel approach that integrates a nanostructured antireflection layer with an interference based ARC. Fig. 1 illustrates this hybrid moth-eye approach, showing the cross-sectional structure and correlated effective index of refraction for the design.

Because the nanostructures are placed in a low-loss layer, this configuration will not lead to significant absorption. Furthermore, this design does not modify any active layers of the underlying cell, and is therefore compatible with any multi-junction design that currently uses thin-film antireflection coatings.

The interference based ARC layers serve the purpose of minimizing reflections between a lower index moth-eye coupling layer and the higher index active layers. This approach allows for a notable improvement over the best multilayer ARCs in a configuration that is compatible with photovoltaic design.

II. OPTICAL MODELING

Optical modeling was performed for 3-J and 4-J designs to compare the hybrid moth-eye ARC to more conventional approaches. The transfer-matrix method was used to calculate the reflectance of various multilayer configurations. This data was then weighted to the AM1.5D spectrum, and the layer structure for each coating was optimized to minimize reflected power in the solar spectrum.

A. Modeling Details

The same principles involved in conventional ARC design apply to the hybrid moth-eye approach. Typically, multiple thin-film layers consisting of low loss materials, such as SiO_2 , Al_2O_3 , Ta_2O_5 , or TiO_2 , are deposited onto the top of the device. Reflection is suppressed due to interference effects between the partial reflections from each interface.

Since the solar spectrum is not flat and covers a very broad range of wavelengths, the design is complex and non-intuitive. To optimize the thickness of each layer, it is necessary to vary the widths until a merit function describing the quality of the design is minimized. Under the simplifying assumption that the internal quantum efficiency (IQE) of the device is unity for all wavelengths larger than the bandgap of the bottom junction, the merit function is described by (1):

$$F = \left(\frac{1}{m} \sum_{j=1}^m |I_j C_j|^k \right)^{1/k} \quad (1)$$

Where m is the number of targets used when summing across a given wavelength range, C is the reflectance calculated using the transfer-matrix method, I is a weighting function that describes the power in the AM1.5D spectrum, and k is the power of the method. [9]

When the power of the method is 1, the merit function simplifies to the AM1.5D weighted average reflectance over the range where the device is absorbing. This optimization will minimize the total power reflected from the device, thereby maximizing the amount of energy coupled into the active layers. As the power of the method increases, larger deviations inside the sum of the merit function are given more weight. This will cause the reflected power spectrum to flatten, which is beneficial when current matching is essential and there is little flexibility for bandgap tuning. For each of our designs, we set the power of the method to 1 so the ARCs will optimize for minimum reflected power.

Many practical considerations must also be taken into account when designing an ARC for a multi-junction device. Some examples include current matching constraints, losses due to the bandgap – open circuit voltage ($E_g/q - V_{oc}$) offset for each junction, and real-world non-unity IQEs.

B. ARC Design Parameters

The design of a hybrid moth-eye ARC is compared to a multilayer ARC, a 2-layer ARC, and no ARC for 3-J and 4-J designs. It is important to constrain each approach to the same parameter space so a fair comparison can be made.

The wavelength range used for optimization was adjusted for a 3-J case and a 4-J case. A low wavelength cutoff of 300 nm is used for both designs since shorter wavelength light makes up an insignificant amount of the total power in the direct spectrum.

For the 3-J range, we assume a bottom junction with a bandgap of 1.0-eV since this is similar to what is used in the highest efficiency 3-J device architectures. This corresponds to a high wavelength cutoff of 1240 nm. [10]

For the 4-J range, we assume a bottom junction made of 0.66-eV germanium, corresponding to a long wavelength cutoff of 1879 nm. It would be difficult to incorporate a material with a lower bandgap into a multi-junction device because there is less energy available at longer wavelengths and the efficiency of the junction would be low due to $(E_g/q - V_{oc})$ offset losses.

Fig. 2 shows the AM1.5D spectrum and illustrates the wavelength ranges used for the 3-J and 4-J cases.

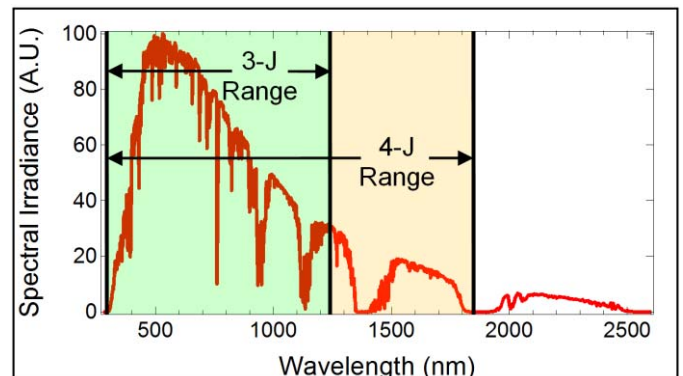


Fig. 2. Plot of the AM1.5D spectrum, showing the relevant high and low wavelength cutoffs used for 3-J and 4-J ARC design.

Material constraints are also important when comparing the design of each ARC. For the interference based ARC layers, SiO_2 and TiO_2 are used. Due to their low ($n \approx 1.5$ for SiO_2) and high ($n \approx 2.7$ for TiO_2) indices of refraction, ARCs consisting of alternating layers of these two materials usually outperformed other combinations. [11]

For the hybrid ARC, we assume that the moth-eye antireflection layer is made of SiO_2 and does not reflect or scatter. This assumption is based on previous reports of near-

TABLE I
ANTIREFLECTION COATING COMPARISONS

ARC Type	3-Junction Range (300 nm-1240 nm)		4-Junction Range (300 nm-1879 nm)	
	757.5 W/m ² in the AM1.5D Spectrum		860.0 W/m ² in the AM1.5D Spectrum	
	Reflected Power (W/m ²)	% of Power Reflected	Reflected Power (W/m ²)	% of Power Reflected
No ARC	232.9	30.7%	260.3	30.3%
2-Layer	38.8	5.1%	55.4	6.4%
Multilayer (4-Layer)	16.5	2.2%	26.5	3.1%
Hybrid Moth-Eye	4.7	0.6%	8.4	1.0%

perfect broadband reflectance into glass using anti-reflective nanostructures. The interference-based antireflective layers are then designed to minimize reflection using SiO₂ as the incident medium. [12]

All the ARCs were optimized to minimize AM1.5D reflected power into indium gallium phosphide (InGaP). This material was chosen because it is used as the top junction for most 3-J and 4-J device architectures. While a multi-junction device has a much more complicated layer structure, we find that minimizing reflection into the top layer will yield a very similar design to a model that takes into account the entire optical structure. Furthermore, this simple comparison should highlight the quality of each approach in a general manner. The relative performance of each design should carry over for devices that incorporate different materials in the ARC and epitaxial structure.

All of the optical constants used for these models were obtained from the Sopra optical database. TFCalc from Software Spectra was used to design the layer structure for each optical coating. Additional information on thin-film ARCs can be found elsewhere. [9][13]

C. Antireflection Coating Comparison

The 3 designs were first optimized to minimize reflected power in the AM1.5D spectrum using the procedures detailed above. At each wavelength, the reflectance is multiplied by the power density in the AM1.5D spectrum to obtain a plot of reflected power vs. wavelength. This plot is shown in Fig. 3 for each ARC design optimized to the 4-J wavelength range.

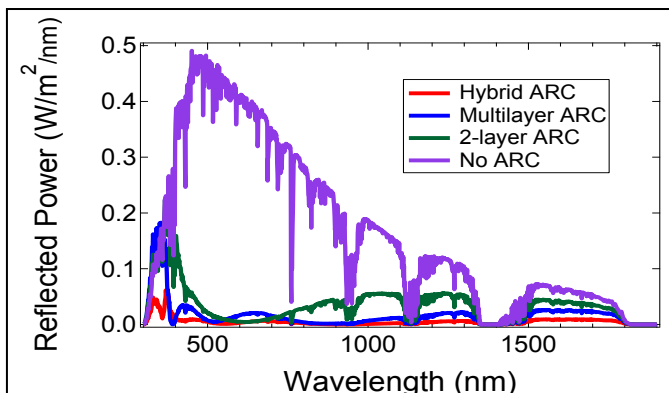


Fig. 3. Plot showing the reflected power vs. wavelength for each of the ARC designs for the 4-J wavelength range.

Summing across the 3-J and 4-J wavelength range allows us to calculate the total reflected power for each design. These results are summarized in Table 1.

For both the 3-J and 4-J ranges, there is a decrease in the reflected power of approximately 3% when comparing a 2-layer ARC to a multilayer ARC. An additional reduction in reflected power of approximately 2% can be obtained by using a hybrid ARC.

It is important to note that the largest improvements occur when optimizing to the 4-J range. This indicates that the more advanced coatings have better broadband characteristics, and should provide greater improvements to 4-J devices than they would to current 3-J designs.

Many important features from each design are also illustrated in the reflected power spectrum in Fig. 3. For the 2-layer ARC, there is a region of very low reflected power centered near 600 nm. However, the region of low reflectivity is not very wide for this design, leading to a high power reflection at short and long wavelengths.

Increasing the power of the method will add weight to regions of the curve with high reflected power, and may help a 2-layer ARC cover a broad wavelength range. However, there are limits to the width of the passband for any 2-layer design, leading to an imbalance in the reflected power spectrum that may have a negative effect on device performance.

A multilayer ARC improves broadband performance because additional layers help to expand the design space. The optimal design consists of just 4 alternating layers of TiO₂ and SiO₂, and allows for a notable reduction in reflected power for blue and infrared wavelengths compared to the 2-layer ARC. Given its simplicity and potential for high performance, a 4-layer ARC is an appealing approach for multi-junction design.

The highest performing design is the hybrid moth-eye ARC. Historically, optical coating design is constrained by the lack of materials with an index of refraction lower than MgF₂ ($n \approx 1.38$). By bridging the refractive index gap between air and SiO₂, the moth-eye coupling layer eliminates this constraint and opens up the potential for higher quality designs.

Compared to the optimized 4-layer ARC, the hybrid approach further decreases reflected power by about 2% across the entire 4-J range. The design is optimized when seven interference-based layers are used, indicating that the added performance comes at the expense of increased complexity, at least during the initial stages of optical design.

III. RESULTS AND DISCUSSION

To validate the optical modeling, each ARC design is placed on a sample consisting of approximately 1 μm of InGaP on a GaAs substrate. The reflectance of the resulting coatings are measured and compared to simulations.

It is important to note that the optical constants reported in the Sopra optical database are not universal to each material. Of particular importance to our design, we find that the measured refractive index of our InGaP layer is a few percent higher and the refractive index of our TiO_2 film is a few percent lower than the values reported. For this reason, it is necessary to carefully characterize each material and re-optimize the designs prior to depositing ARCs.

A. Experimental Details

Approximately 1 μm of InGaP was first grown on a GaAs substrate using MOCVD. The optical constants and thickness of the InGaP layer was measured using ellipsometry. The SiO_2 and TiO_2 interference-based ARC layers were deposited using a VEECO Ion Beam Assisted Sputter Deposition system. The optical constants and deposition rate for each film were also characterized using ellipsometry. Each design was then re-optimized using updated material parameters.

The final layers for each of the 3 ARCs were deposited onto each sample. For the hybrid design, an additional layer of SiO_2 was deposited with a thickness of approximately 1.5 μm to accommodate the moth-eye coupling layer. This thickness should not have an effect on reflectance as long as the nanostructures exhibit good antireflective properties.

Thermal nanoimprint lithography was then used to transfer the moth-eye pattern from a nickel master stamp to a thin thermoplastic polymer on top of the sample. The nickel stamp was fabricated by NIL Technology and the imprinting of the overlying resist layer was done using a Nanonex imprinting tool. The imprint was carried out at a pressure of 450 psi and a temperature of 140°C.

Fig. 4a shows a cross sectional SEM of a hybrid ARC after the imprinting process. The period and height of the moth-eye structure is about 350 nm.

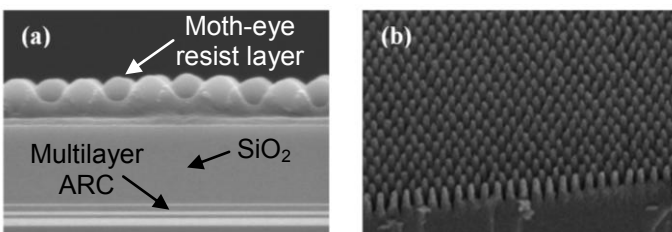


Fig. 4. (a) Cross sectional SEM of the hybrid moth-eye design showing a multilayer ARC and imprinted moth-eye layer. (b) SEM of sample showing excellent replication of moth-eye pattern.

The pattern is transferred into the SiO_2 layer using an Inductively Coupled Plasma (ICP) etch. It is possible to

control the aspect ratio by adjusting etch parameters to change the selectivity of SiO_2 to the thermoplastic. We achieve a selectivity of roughly 1.7 using a 300W CHF_3 etch. This leads to an increased aspect ratio for the final moth-eye pattern, which is beneficial to its antireflective properties.

After transferring the moth-eye pattern into the SiO_2 coupling layer, the remaining thermoplastic is removed with acetone and the design is complete. Fig. 4b shows the sample after the ICP etch and with the resist layer removed. Note the increased aspect ratio of the moth-eye structures.

B. Results

Specular reflectance for each ARC was measured using a Cary 500 UV-VIS-NIR Spectrophotometer. These reflectance scans are compared to optical models.

Fig. 5 shows this comparison for each design. The simulations take into account the interface between InGaP and GaAs. This interface is responsible for the interference fringes that begin around 675 nm, corresponding to the bandgap of InGaP. The period of these fringes is linked to the InGaP layer thickness.

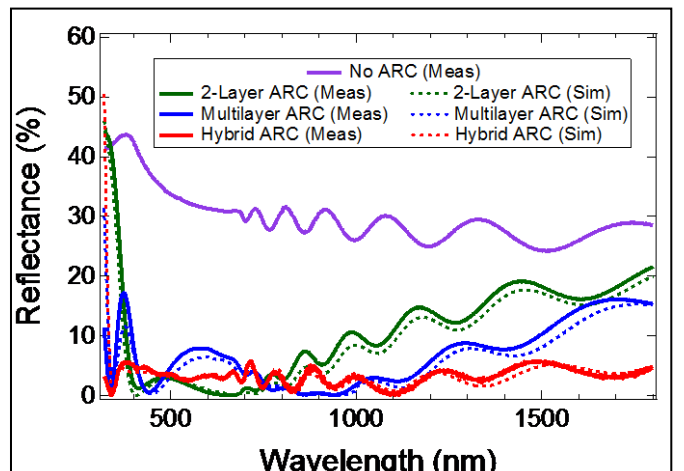


Fig. 5. Plot showing the measured and simulated reflectance for each ARC design

Each design has very distinctive characteristics. The 2-layer ARC exhibits excellent performance for short wavelengths, having the lowest reflectance of all the designs from about 500-850 nm. At this point, the reflectance begins to rise steadily to more than 20% at 1800 nm. The 4-layer ARC has better IR performance, but there remains a steady increase in reflectivity beyond 1100 nm. The hybrid ARC exhibits the best broadband characteristics and maintains a very low reflectance across the entire 4-J range.

Since the merit function is weighted to the direct spectrum, a measure of the reflected AM1.5D power should provide a good comparison between each design. Using this metric, we find that the hybrid ARC performs significantly better than the other 2 designs. The 2-layer ARC reflects 47.4 W/m^2 , corresponding to 5.5% of the AM1.5D power in the 4-J

wavelength range. The 4-layer ARC reflects 38.6 W/m^2 , or 4.5% of the power in the 4-J range. In comparison, the hybrid ARC reflects just 23.9 W/m^2 , corresponding to a 2.8% power reflection.

There is excellent agreement between the simulated and measured reflectance for each design. This is a particularly significant result for the hybrid ARC since the simulation calculates the reflectance of the multilayer structure using SiO_2 as the incident medium. This assumption is only valid when the moth-eye layer is not reflecting, absorbing, or scattering a considerable amount of light.

If the nanostructures were significantly absorbing or scattering, we would see a negative vertical offset in the measured specular reflectance. If the nanostructures were reflecting a substantial amount of light, we would have to insert additional elements into the transfer matrix when calculating the reflection coefficient; causing the spectrum to modulate. However, no modulation or offset is observed when comparing the two curves.

The excellent agreement between theoretical and measured reflectance is therefore an indication that the antireflective nanostructures are effectively coupling light into the top SiO_2 layer as expected.

IV. CONCLUSIONS

In this work, we present a novel ARC design which integrates a moth-eye antireflection layer with a multilayer dielectric stack. This approach is compared to multilayer and 2-layer ARC designs. Optical models show that an optimized hybrid ARC can reduce the reflected AM1.5D power by 10-45 W/m^2 over a 2-layer and multilayer ARC. Furthermore, they exhibit better broadband characteristics compared to conventional multilayer designs. This is very important for 4-J devices that absorb to longer wavelengths than current state-of-the-art 3-J cells.

The three ARCs were fabricated on a sample consisting of approximately 1 μm of InGaP on GaAs. The measured reflectance for each coating shows that the hybrid ARC can reduce the reflected AM1.5D power by 2 to 3% compared to 2-layer and multilayer thin-film designs. This translates into an improvement of roughly 1% in cell efficiency for a 40% efficient multi-junction device.

Furthermore, there is an excellent agreement between the modeled and measured reflectance, indicating that the replicated moth-eye layer is exhibiting excellent antireflection properties with minimal absorption and scattering.

ACKNOWLEDGEMENTS

This material is based upon work supported as part of the Center for Energy Efficient Materials (CEEM), an Energy Frontier Research Center (EFRC) funded by the U.S. Department of Energy, Office of Science, Office of Basic Energy Sciences under Award Number DE-SC0001009.

Part of this work is done in University of California, Santa Barbara Nanofabrication Facility, supported by the National Science Foundation and the National Nanofabrication Infrastructure Network (NNIN).

Emmett E. Perl is supported by the National Science Foundation Graduate Research Fellowship under Grant No. DGE-1144085.

We thank Alan Kibbler for assistance with the epitaxial growth of the InGaP/GaAs samples, and Brian Thibeault for helping to develop the fabrication process.

REFERENCES

- [1] Green, Martin A., Keith Emery, Yoshihiro Hishikawa, Wilhelm Warta, and Ewan D. Dunlop. "Solar cell efficiency tables (version 41)." *Progress in Photovoltaics: Research and Applications* 21, no. 1(2013): 1-11.
- [2] Law, Daniel C., R. R. King, H. Yoon, M. J. Archer, A. Boca, C. M. Fetzer, S. Mesropian et al. "Future technology pathways of terrestrial III-V multijunction solar cells for concentrator photovoltaic systems." *Solar Energy Materials and Solar Cells* 94, no. 8 (2010): 1314-1318.
- [3] Aiken, Daniel J. "High performance anti-reflection coatings for broadband multi-junction solar cells." *Solar energy materials and solar cells* 64, no. 4 (2000): 393-404.
- [4] King, R. R., A. Boca, W. Hong, X. Q. Liu, D. Bhusari, D. Larrabee, K. M. Edmondson et al. "Band-gap-engineered architectures for high-efficiency multijunction concentrator solar cells." In 24th European Photovoltaic Solar Energy Conference and Exhibition, Hamburg, Germany, vol. 21. 2009.
- [5] Geisz, John F., J. Scott Ward, Anna Duda, Waldo Olavarria, Lynn Gedvilas, Michelle Young, Mark W. Wanlass et al. "Infrared Reflective and Transparent Inverted Metamorphic Triple Junction Solar Cells." In *AIP Conference Proceedings*, vol. 1277, p.11. 2010.
- [6] C.G. Bernhard; "Structural and Functional Adaptation in a Visual System." *Endeavor*, 26 (1967), p. 79
- [7] Wilson, S. J., and M. C. Hutley. "The optical properties of moth eye antireflection surfaces." *Journal of Modern Optics* 29, no. 7 (1982): 993-1009.
- [8] Tommila, J., V. Polojärvi, A. Aho, A. Tukiainen, J. Viheriälä, J. Salmi, A. Schramm et al. "Nanostructured broadband antireflection coatings on AlInP fabricated by nanoimprint lithography." *Solar Energy Materials and Solar Cells* 94, no. 10 (2010): 1845-1848.
- [9] TFCalc Version 3.5.15 User's Manual, Software Spectra, Inc., (2009).
- [10] Geisz, John F., Anna Duda, Ryan M. France, Daniel J. Friedman, Ivan Garcia, Waldo Olavarria, Jerry M. Olson, Myles A. Steiner, J. Scott Ward, and Michelle Young. "Optimization of 3-junction inverted metamorphic solar cells for high-temperature and high-concentration operation." In *AIP Conference Proceedings*, vol. 1477, p. 44. 2012.
- [11] Macleod, Hugh Angus. *Thin film optical filters*. Taylor & Francis, 2001.
- [12] Hobbs, Douglas S., Bruce D. MacLeod, and Juanita R. Riccobono. "Update on the Development of High Performance Anti-Reflecting Surface Relief Micro-Structures." *SPIE 6545-34* (2007).
- [13] Database of Refractive Indices for Different Materials [electronic resource], <http://refractiveindex.info>, accessed June. 8, 2013.